

# Numerical simulation of turbulent sediment transport, from bed load to saltation.

Orencio Durán,<sup>1, a)</sup> Bruno Andreotti,<sup>1</sup> and Philippe Claudin<sup>1</sup>

*Physique et Mécanique des Milieux Hétérogènes, (PMMH UMR 7636 ESPCI – CNRS – Univ. Paris-Diderot – Univ. P. M. Curie), 10 rue Vauquelin, 75005 Paris, France*

(Dated: 15 October 2022)

Sediment transport is studied as a function of the grain to fluid density ratio using two phase numerical simulations based on a discrete element method (DEM) for particles coupled to a continuum Reynolds averaged description of hydrodynamics. At a density ratio close to unity (typically under water), vertical velocities are so small that sediment transport occurs in a thin layer at the surface of the static bed, and is called bed load. Steady, or ‘saturated’ transport is reached when the fluid borne shear stress at the interface between the mobile grains and the static grains is reduced to its threshold value. The number of grains transported per unit surface is therefore limited by the flux of horizontal momentum towards the surface. However, the fluid velocity in the transport layer remains almost undisturbed so that the mean grain velocity scales with the shear velocity  $u_*$ . At large density ratio (typically in air), the vertical velocities are large enough to make the transport layer wide and dilute. Sediment transport is then called saltation. In this case, particles are able to eject others when they collide with the granular bed, a process called splash. The number of grains transported per unit surface is selected by the balance between erosion and deposition and saturation is reached when one grain is statistically replaced by exactly one grain after a collision, which has the consequence that the mean grain velocity remains independent of  $u_*$ . The influence of the density ratio is systematically studied to reveal the transition between these two transport regimes. Based on the mechanisms identified in the steady case, we discuss the transient of saturation of sediment transport and in particular the saturation time and length. Finally, we investigate the exchange of particles between the mobile and static phases and we determine the exchange time of particles.

## I. INTRODUCTION

After the pioneering works of Richardson<sup>1</sup>, Rouse<sup>2</sup> and Vanoni<sup>3</sup>, transport and dispersion of impurities suspended in turbulent flows, such as sand grains, dust, bubbles or droplets, have received a renewed interest in the last decade, both from the fundamental point of view<sup>4–6</sup> and for its applications to planetology<sup>7</sup>, cloud physics<sup>8</sup> and geomorphology. In the later case, sediment may be entrained, transported and deposited by water flow or by wind. Then, gravity cannot be neglected as transport usually takes place in a turbulent boundary layer bounded by an erodible granular bed. Moreover, transported particles are not passively advected by the flow: they induce a negative feedback, which eventually limits the erosion of the granular bed, leading to a steady state in which erosion and deposition balance each other.

In such a homogeneous and steady situation, the fluid flow can be characterized by a unique quantity: the shear velocity  $u_*$ . The flux of sediments transported by the flow, called the saturated flux and noted  $q_{\text{sat}}$ , is an increasing function of  $u_*$  whatever the nature of the fluid. For aeolian transport, there has been great effort to obtain the relation  $q_{\text{sat}}(u_*)$  experimentally<sup>9–19</sup> using both wind tunnels and atmospheric flows in the

field, numerically<sup>20–24</sup> and theoretically<sup>10,25–31</sup>. Similarly, several expressions for subaqueous bed-load have been proposed,<sup>32–39</sup>. Most models are based on the same dynamical mechanisms and differ only by the approximation used to compute the particle trajectories<sup>40–44</sup>. For this reason, experiments have been performed to determine the saltating motion of individual particles under water<sup>45–49</sup> and in air<sup>50–53</sup>.

Despite this wide literature, some fundamental aspects of sediment transport are still only partly understood. For instance, the dynamical mechanisms limiting sediment transport, in particular the role of the bed disorder<sup>54</sup> and turbulent fluctuations<sup>55–62</sup>, remain a matter of discussion. Also, derivations of transport laws have a strong empirical or semi-empirical basis, thus lacking more physics-related inputs. Here we investigate the properties of sediment transport using a novel numerical description of particle-laden flows. In particular, we examine the transition from bed-load to saltation by studying the influence of the grain to fluid density ratio.

In section II, we introduce the equations of motion for the grains as well as the equations of hydrodynamics, emphasizing the coupling between the two. Then, in section III, we detail the characteristics of saturated transport in the two limiting cases: bed load (water) and saltation (air). In section IV, we propose an interpretation of the simulations based on simple transport models. We then use these transport descriptions to derive and discuss out-of-equilibrium transport and in particular the saturation length and time (section V). We contrast this

<sup>a)</sup>present address: Univ N Carolina, Dept Geol Sci, 104 South Rd, Mitchell Hall, Campus Box 3315, Chapel Hill, NC 27515 USA.

time with the ‘exchange time’, which characterizes the diffusion of particles through the static/mobile interface. Finally, conclusions are outlined in the last section.

## II. TRANSPORT MODEL

### A. Key ideas

We wish to model the transport of non-cohesive grains by a flow, under gravity. Although a continuum ‘two phase’ (grains and fluid) modeling<sup>63</sup> is very appealing, it is problematic by several aspects. (i) It postulates that particles constitute an Eulerian phase, which means that the particles crossing an arbitrary control volume have almost the same velocity. In a homogeneous steady flow, an Eulerian approach immediately predicts that particles are transported along the direction parallel to the bed and to the flow – vertical velocities are ignored. However, at least for saltation, they are essential. (ii) Such a continuum approach ignores the discrete and disordered nature of the granular phase. However, these properties are essential close to the transport threshold, below which no grain can be entrained. Such models incorrectly predict the threshold shear velocity and in particular its strong decrease with the grain Reynolds number. To avoid these issues, we use here a discrete element method for the particles<sup>20–22</sup>.

Resolving hydrodynamics around grains is technically feasible only if the size of the domain (the number of grains) and the time over which the simulation is run are very small. The idea introduced here is thus to use a continuum description of hydrodynamics, averaged at a scale larger than the grain size. This means that the feedback of the particles on the flow is treated in the mean field manner.

This method allows one to perform very long numerical simulations (typically  $1000 \sqrt{d/g}$ , using large spatial domains (typically  $1000 \times 15$  grains), while keeping the complexity of the granular phase. We will now detail the different ingredients of the model. To avoid the formation of ordered structures in the grain packing, we have used a slightly polydisperse sample (20%). For the sake of simplicity, we only give here the equations for the strictly monodisperse case (grains of diameter  $d$ ).

### B. Forces on particles

#### 1. Equations of motion

The grains have a spherical shape and are described by their dimensionless position vector  $\vec{r}$ , velocity  $\vec{u}$  and angular velocity  $\vec{\omega}$ . A given grain labelled  $p$  inside a fluid

obeys the equations of motion,

$$m \frac{d\vec{u}^p}{dt} = -m \left( 1 - \frac{\rho_f}{\rho_p} \right) g \vec{e}_z + \sum_q \vec{f}_{p,q} + \vec{f}_{\text{drag}}^p$$

$$I m d \partial_t \vec{\omega}^p = \frac{1}{2} \sum_q \vec{n}_{p,q} \times \vec{f}_{p,q} \quad (1)$$

where  $\vec{e}_z$  is the vertical unit vector,  $I = 1/10$  is the normalized moment of inertia of a sphere,  $\vec{f}_{p,q}$  is the contact force with grain  $q$ ,  $\vec{n}_{p,q} = (\vec{r}^q - \vec{r}^p) / |\vec{r}^q - \vec{r}^p|$  is the contact direction and  $\vec{f}_{\text{drag}}^p$  is the drag force.

#### 2. Contact forces

Following a standard approach for the modeling of contact forces in MD codes, see<sup>64–67</sup> and references therein, we consider the case where grains in contact are subject to (i) normal repulsion, (ii) tangential friction and (iii) energy dissipation. For simplicity, the normal repulsion is given by a spring-like elastic force, which is a good approximation for very small contact deformations. The tangential friction is modeled by a tangential elastic force proportional to the relative tangential displacement between the grains. The moment of this force can induce particle rotation. Whenever the tangential exceeds a given fraction of the normal force, defined by a microscopic friction coefficient, the contact ‘slides’ (Coulomb friction law). Finally, energy dissipation at the contact is ensured by adding a damping term to the force, proportional to the relative contact velocity. This term accounts for the restitution coefficient  $e$ , i.e. the ratio between grain velocities after and before a collision.

#### 3. Drag force

We hypothesize here that the drag force exerted by the fluid on a moving grain only depends on the difference between the grain velocity  $\vec{u}^p$  and the fluid velocity  $\vec{u}$  around it. This assumption is valid if the turbulent fluctuations of the flow itself can be neglected in front of those induced by the grain. Introducing the particle Reynolds number  $R_u$  based on this fluid-particle velocity difference  $R_u = |\vec{u} - \vec{u}^p| d / \nu$ , the drag force can be written under the form

$$\vec{f}_{\text{drag}}^p = \frac{\pi}{8} \rho_f d^2 C_d(R_u) |\vec{u} - \vec{u}^p| (\vec{u} - \vec{u}^p) \quad (2)$$

where  $C_d(R_u)$  is the drag coefficient. We use the following convenient phenomenological approximation<sup>68</sup>:

$$C_d(R_u) = \left( \sqrt{C_d^\infty} + \sqrt{R_u^c / R_u} \right)^2 \quad (3)$$

where  $C_d^\infty \simeq 0.5$ , is the drag coefficient of the grain in the turbulent limit ( $R_u \rightarrow \infty$ ), and  $R_u^c \simeq 24$  is the transitional particle Reynolds number above which the drag

coefficient becomes almost constant. The lift force and the corrections to the drag force (Basset, added-mass, etc.) are neglected.

### C. Hydrodynamics

Hydrodynamics is described by the Reynolds averaged Navier-Stokes equations:

$$\rho_f (\partial_t u_i + u_j \partial_j u_i) = -\partial_i p + \rho_f g_i + \partial_j \tau_{ij}^f - F_i. \quad (4)$$

In this expression,  $\tau_{ij}^f$  is the total stress tensor resulting both from viscous diffusion of momentum (viscous stress) and transport of momentum by turbulent fluctuations (Reynolds stress).  $F_i$  is the body force exerted by the grains on the fluid. It reflects the turbulent fluctuations induced by a moving grain, which can be non-local. As we focus in this paper on steady homogeneous sediment transport, we hypothesize that the influence of a given grain remains localized in a thin horizontal region and that the typical horizontal distance over which the flow is disturbed is comparable to the distance between moving grains.  $F_x(z)$  can then be obtained by averaging the horizontal component of the drag  $f_{\text{drag } x}^p$  acting on all the grains moving around altitude  $z$ , in a horizontal layer of area  $A$  and of thickness  $dz$ :

$$F_x(z) = \frac{1}{Adz} \left\langle \sum_{p \in \{z; z+dz\}} f_{\text{drag } x}^p(z) \right\rangle. \quad (5)$$

The  $\langle \cdot \rangle$  denote here the ensemble averaging. In order to gain statistics, we make use of the steady character of the studied situation, and also use time averaging. For simplicity, we note  $\tau^f = \tau_{xz}^f$  the fluid shear stress, and  $u = u_x$  for the fluid horizontal velocity. The horizontal component of the Reynolds equation reduces to  $\partial_z \tau^f = F_x$ , which can be integrated in

$$\tau^f(z) = \rho_f u_*^2 - \tau^p(z) \quad (6)$$

where we have introduced the shear velocity  $u_*$  and the grain borne shear stress  $\tau^p$  thus defined by

$$\tau^p(z) \equiv \int_z^\infty dz' F_x(z') = \frac{1}{A} \left\langle \sum_{p \in \{z' > z\}} f_{\text{drag } x}^p(z') \right\rangle. \quad (7)$$

In order to relate the fluid borne shear stress to the average velocity field, we adopt Prandtl's turbulent closure<sup>69</sup>. Introducing the turbulent mixing length  $\ell$ , we write

$$\tau^f = (\nu + \ell^2 |\partial_z u|) \partial_z u \quad (8)$$

We know that  $\ell$  should vanish below some critical Reynolds number  $R_c$  and should be proportional to the distance to the ground  $z$ , far above the transport layer.

TABLE I. Units used in the model, expressed in terms of the grain density ( $\rho_p$ ), fluid density ( $\rho_f$ ), gravity ( $g$ ) and mean grain diameter ( $d$ )

General	
length $l$	$d$
acceleration	$g$
time $t$	$\sqrt{d/g}$
velocity $v$	$\sqrt{gd}$
Particles	
angular velocity $\omega$	$\sqrt{g/d}$
mass $m$	$\frac{\pi}{6} \rho_p d^3$
moment of inertia $I$	$md^2$
force $f$	$mg$
contact stiffness $k$	$mg/d$
damping constant $\gamma$	$m\sqrt{g/d}$
Fluid	
shear stress $\tau$	$(\rho_p - \rho_f)gd$

We have used a phenomenological differential equation to formulate the mixing length

$$\frac{d\ell}{dz} = \kappa \left[ 1 - \exp \left( -\sqrt{\frac{1}{R_c}} \left( \frac{u\ell}{\nu} \right) \right) \right] \quad (9)$$

where  $\kappa \simeq 0.4$  is von Karman's constant. Here  $R_c$  is fixed to 17. The ratio  $u\ell/\nu$  is the Reynolds number based on the mixing length. Note that a function other than the exponential can also be used, provided it has the same behavior in 0 and  $-\infty$ . This formulation allows us to define  $\ell$  both inside and above the static granular bed. Interestingly, there is no need to explicitly define an interface between static and mobile zones.

### D. Dimensionless numbers

As is the case in any numerical simulation, the equations are made dimensionless. Gravity gives the relevant scale for forces. More precisely, it only appears in the grain equation of motion under the form of a buoyancy-free gravity  $\left(1 - \frac{\rho_f}{\rho_p}\right)g$ . The choice of the typical length scale is less obvious. On one hand, the contact forces and the trapping of particles at the surface of the bed do not depend on the fluid properties: the grain diameter  $d$  is thus the relevant length scale for the static grains. On the other hand, one can build a drag length from hydrodynamics, which is the length needed to accelerate a grain to the fluid velocity. This inertial length scales as  $\frac{\rho_p}{\rho_f}d$  and is the relevant length scale for the mobile grains. This means that the density ratio  $\rho_p/\rho_f$  cannot be eliminated and is a true dimensionless parameter of the problem. We shall see below that this density ratio is the parameter controlling the transition from bed load to saltation. We have chosen  $d$  as a reference length scale, and Table I summarizes all the parameters used to make

the problem dimensionless in our code. The second control parameter is the shear velocity  $u_*$  imposed far from the bed, or equivalently the shear stress  $\rho_f u_*^2$ . Its dimensionless counterpart is the Shields number<sup>70</sup>, defined by

$$\Theta = \frac{\rho_f u_*^2}{(\rho_p - \rho_f)gd}, \quad (10)$$

which encodes the strength of the flow. Making the viscosity non-dimensional, we obtain a grain-based Reynolds number

$$Re = \frac{d}{\nu} \sqrt{\left(\frac{\rho_p}{\rho_f} - 1\right)gd} \quad (11)$$

Physically, it determines the hydrodynamic regime at the scale of the grain. The figures presented in this paper are obtained using the same particle Reynolds number  $Re = 10$ . This value is sufficiently large to ensure that the grain diameter is much larger than the viscous sub-layer size. As a consequence, the flow is fully turbulent at all the scales of the problem. It becomes viscous below the first layer of static grains.

Dynamics at the scale of the contact between grains is controlled by other numbers: the restitution coefficient  $e$ , the friction coefficient  $\mu$  and the contact duration  $t_c = \pi \sqrt{\frac{g}{(2k - \gamma^2)d}}$  (in terms of the contact stiffness  $k$  and the damping constant  $\gamma$ <sup>65</sup>). We have checked that the values given to these parameters do not qualitatively change the results.

### III. SATURATED TRANSPORT

#### A. Qualitative results

Transport equations are integrated until a statistically steady homogeneous state is reached. Since we are primarily interested in the transition from bed load to saltation, we have varied the Shields number within the range  $\Theta = 0.003$ – $0.5$  (a range which contains the threshold  $\Theta_d$ , see below) and the density ratio within the range  $\rho_p/\rho_f = 2$ – $2000$ .

Once transport has reached its saturated state, the general picture is as follows: at small density ratios  $\rho_p/\rho_f \simeq 2$ , which is the typical value under water, the transport is confined at the surface, within a few grain diameters. The dense and thin transport layer is characteristic of the bed load regime. On the contrary, at a large density ratio  $\rho_p/\rho_f \simeq 2000$ , which is typical of aeolian situation, the transport layer becomes wide and dilute, extending over several tens of grain diameters (Fig. 1). This is typical of the saltation regime. Within the very same numerical model, we are thus able to reproduce the basic characteristics of transport at both limits.

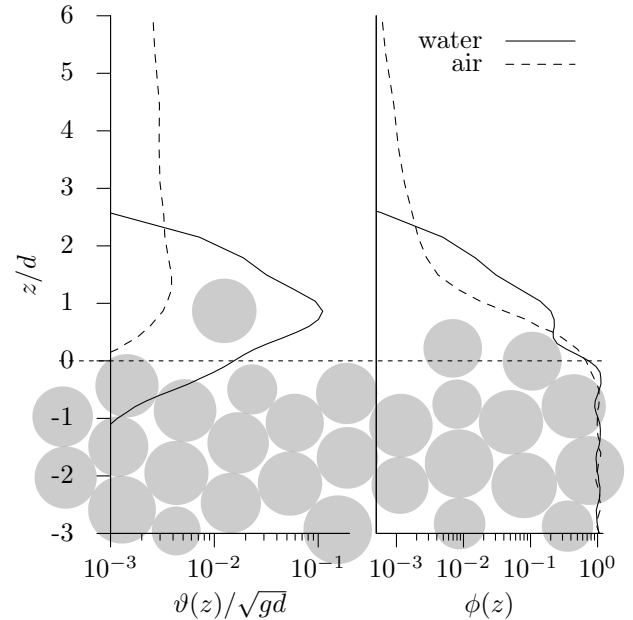


FIG. 1. Transport profiles: volume flux density  $\vartheta(z)$  (left) and volume fraction  $\phi(z)$  (right) for water (solid lines) and air (dashed lines).

#### B. Saturated flux

Steady and homogeneous sediment transport is basically quantified by the volumetric saturated flux  $q_{\text{sat}}$ , i.e. the volume of the particles (at the bed density) crossing a vertical surface of unit transverse size per unit time. It has the dimension of  $\text{m}^2/\text{s}$ . In the simulations, we compute it as

$$q_{\text{sat}} = \frac{1}{A\phi_b} \frac{\pi}{6} d^3 \sum_p u^p, \quad (12)$$

where  $\phi_b$  is the volume fraction of the static bed. A key issue is the dependence of  $q_{\text{sat}}$  on the shear velocity or, equivalently, on the Shields number  $\Theta$ . In order to highlight this dependence, figure 2 shows the saturated flux rescaled by  $u_*^2$  in both cases (water and air). In agreement with experimental observations<sup>19,32–36,39,71–74</sup>, we find that  $q_{\text{sat}}$  scales asymptotically as  $\Theta$  (or  $u_*^2$ ) for saltation, while  $q_{\text{sat}}$  scales as  $\Theta^{3/2}$  (or  $u_*^3$ ) underwater (Fig. 2). Most models of aeolian transport miss the influence of the negative feedback of transport on the flow. Therefore, they do not give the correct scaling, predicting  $q_{\text{sat}} \propto u_*^3$ . We demonstrate below, in the same numerical model, a fundamental difference between the two transport regimes, which correspond to different underlying dynamical mechanisms.

Figure 2 reveals the existence of a threshold shear velocity below which the flux vanishes. More precisely, we define the dynamical threshold Shield number  $\Theta_d$  from the extrapolation of the saturated flux curve to 0, which

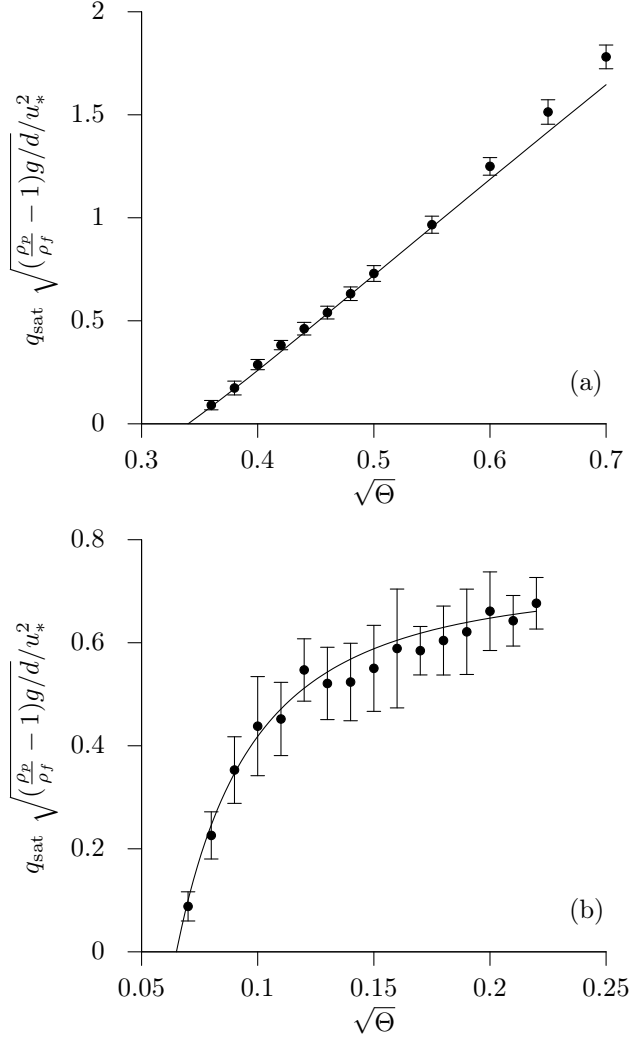


FIG. 2. Rescaled saturated flux  $q_{\text{sat}} \sqrt{(\rho_p/\rho_f - 1)g/d/u_*^2}$  versus the rescaled shear velocity  $\sqrt{\Theta}$  for water (a) and air (b). For air the saturated flux scales asymptotically as  $\Theta$  while for water it follows  $\Theta^{3/2}$ . Full lines are the predictions of the simplified models for bed load (Eq. 24) and saltation (Eq. 30), given in the text.

gives in our case  $\Theta_d \simeq 0.12$  for water ( $\rho_p/\rho_f = 2$ ) and  $\Theta_d \simeq 0.004$  for air ( $\rho_p/\rho_f = 2000$ ), respectively. These values are consistent with experimental ones within a factor of 2. A refined tuning of these values could be achieved by adjusting the value of  $R_c$  and by performing 3D simulations. Figure 3 shows the dependence of the threshold  $\Theta_d$  with the density ratio  $\rho_p/\rho_f$ . It is usually assumed that the Shields number compares directly the horizontal force exerted on a surface grain to its weight, in which case the threshold Shields number could be interpreted as an effective friction coefficient, within a numerical factor. If this was true,  $\Theta_d$  would be a constant, independent of  $\rho_p/\rho_f$ . However, one observes that  $\Theta_d$  decreases rapidly with the density ratio.

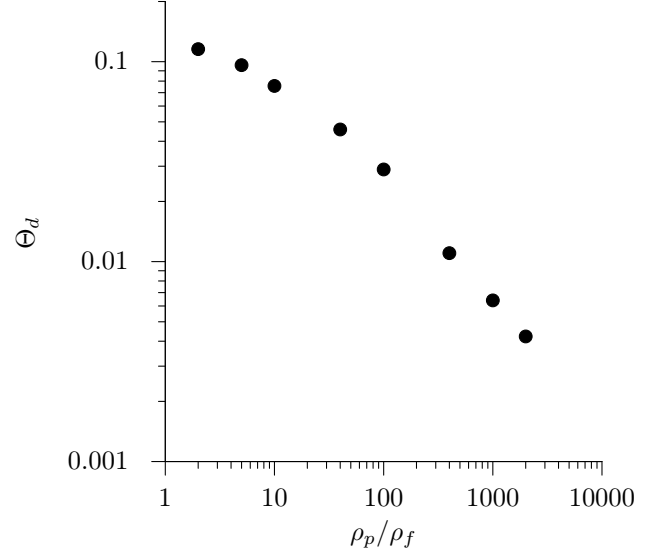


FIG. 3. Dynamical threshold Shield number  $\Theta_d$  as a function of the density ratio  $\rho_p/\rho_f$ .

### C. Transport layer

Figure 4 presents the vertical profiles of the flux density, i.e. the flux per unit height  $\vartheta(z)$  (such that  $q_{\text{sat}} \equiv \int \vartheta(z) dz$ ) for different shear velocities. It shows that bed load and saltation mainly differ by the vertical characteristics of the transport layer. At small density ratios the motion of grains is confined within a thin layer of few grain diameters (Fig. 4 a). Most of the bed load occurs at about one grain diameter above the static bed and the flux density profile decays symmetrically on both sides of this maximum. By contrast, for large density ratios, grains experience much higher trajectories and the transport layer is much wider. Figure 4b shows that the flux density still presents a maximum close to the static bed but decreases exponentially with height.

These qualitative observations can be formalized by defining a characteristic transport layer thickness  $\lambda$  from the flux density profile  $\vartheta(z)$  as:

$$\lambda = \left( \frac{\int_0^\infty (z - \bar{z})^2 \vartheta(z) dz}{q_{\text{sat}}} \right)^{1/2} \quad (13)$$

where  $\bar{z} = \frac{1}{q_{\text{sat}}} \int_0^\infty z \vartheta(z) dz$  gives the altitude of the transport layer centre. If the flux profile decreases exponentially,  $\lambda$  is the characteristic distance over which this decrease takes place. The variations of  $\lambda$  with the shear velocity are presented in the insets of figure 4. For underwater bed load, the size of the transport layer is about one grain diameter, gently increasing with the shear velocity from  $\lambda \simeq d/2$  to  $\lambda \simeq d$ . For aeolian saltation the transport layer is indeed wider, with a characteristic size  $\lambda \simeq 50d$  roughly independent of the shear velocity.

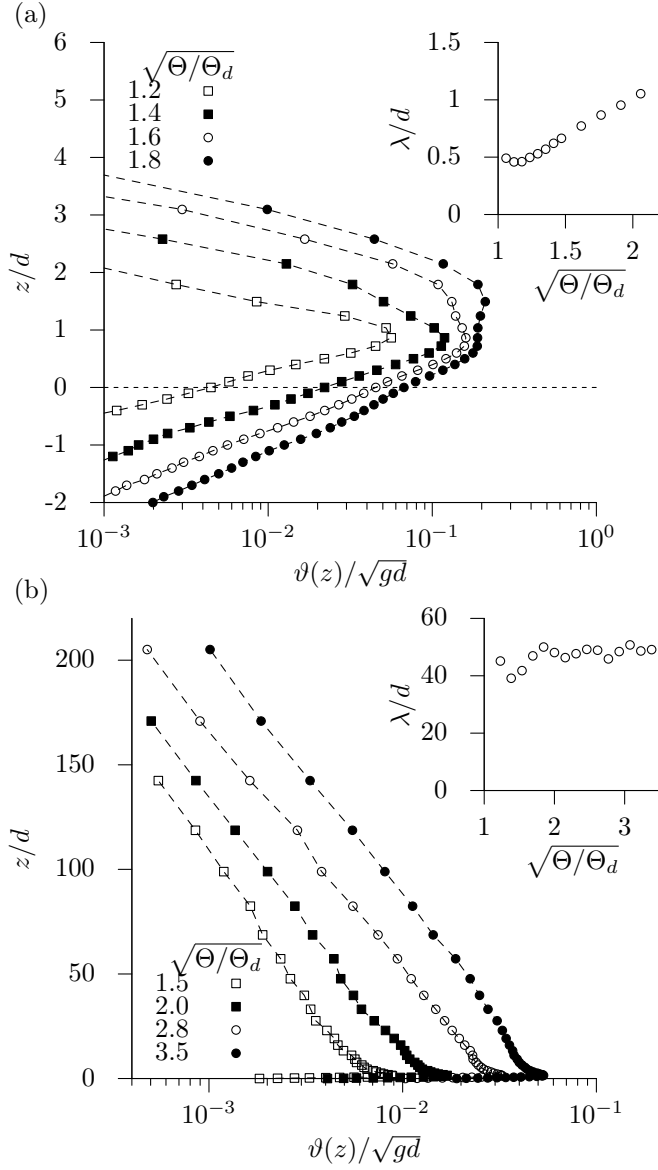


FIG. 4. Vertical profiles of the sediment flux density  $\vartheta(z)$  for different values of the shear velocity ratio  $\sqrt{\Theta/\Theta_d}$ , in water (a) and air (b). The reference height  $z = 0$  denotes the position of the bed surface. Insets: characteristic transport layer thickness  $\lambda$  as function of the shear velocity.

Figure 5 shows the dependence of the transport layer thickness  $\lambda$  with the density ratio. At large density ratios,  $\lambda$  is observed to scale with the drag length  $\frac{\rho_p}{\rho_f}d$  which is the length that naturally emerges when the motion of the grains is dominated by the balance between inertia and hydrodynamical drag. This length is thus expected to control the characteristic hop height and hop length, which naturally leads to wider transport layers for lighter fluids.

Nevertheless, the transition from bed load to saltation is slightly more complex as  $\lambda$  does not strictly obey

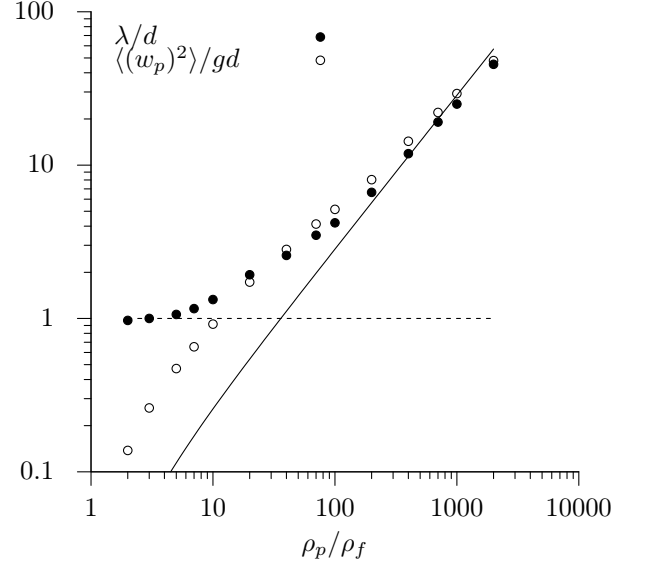


FIG. 5. Characteristic transport layer thickness  $\lambda$  (●) as function of the density ratio for  $\Theta = 2\Theta_d$ . At small density ratios it is limited by the grain size (dashed line), while for large ones it scales as  $\rho_p/\rho_f d$  (solid line). The averaged vertical energy per grain  $\langle (w^p)^2 \rangle / g$  (○) is also shown to illustrate the dynamical origin of  $\lambda$  (see text).

the simple scaling law  $\lambda \propto \frac{\rho_p}{\rho_f}d$ . In sub-aqueous conditions, the transport layer thickness is actually limited by the grain size  $\lambda \sim d$ , which is the characteristic length scale for contact forces and geometrical trapping of particles<sup>75,76</sup>. The hop height can be estimated from the particle vertical velocity  $w^p$  using the ballistic approximation, neglecting the vertical component of the drag force. Under this hypothesis, one expects the hop height to increase like  $(w^p)^2/g$ . Figure 5 shows the dependence of the average squared vertical velocity  $\langle (w^p)^2 \rangle$  on the density ratio. One observes that the transport layer thickness  $\lambda$  is determined by the hop length  $\langle (w^p)^2 \rangle / g$  for  $\rho_p/\rho_f \gtrsim 10$ . Below this cross-over value, the transport layer thickness is given by the grain diameter  $d$ , as trajectories are almost horizontal. The transition from bed load to saltation therefore takes place when the vertical velocities of the particles are sufficiently large for these particles to escape the traps formed by the grains on the static bed. Formally, the criterion of this transition can then be written as  $\langle (w^p)^2 \rangle \simeq gd$ .

#### IV. INTERPRETATION

##### A. A simple transport model for bedload

We propose here a simple model of bed load inspired from Bagnold's original ideas<sup>34</sup>. We hypothesise that moving grains are confined in a thin layer with thickness

on the order of  $d$ . As the average particle vertical velocity is very small, grain hop heights are typically much smaller than  $d$  (Fig. 5), which means that the vertical motion of the grains can effectively be neglected. The saturated flux can then be decomposed as the product of the number  $n$  of transported grains per unit area by the mean grain horizontal velocity  $\bar{u}^p$ :

$$q_{\text{sat}} = \frac{1}{\phi_b} \frac{\pi}{6} d^3 n \bar{u}^p. \quad (14)$$

In the numerical simulations, we compute  $n$  and  $\bar{u}^p$  as

$$n = \frac{\left(\sum_p u_p\right)^2}{A \sum_p u_p^2}, \quad (15)$$

$$\bar{u}^p = \frac{\sum_p u_p^2}{\sum_p u_p}, \quad (16)$$

where  $A$  is the surface area. Notice that these definitions are consistent with the definition of  $q_{\text{sat}}$  (12). If all grains were moving at the same velocity, then  $n$  and  $u^p$  would indeed be respectively the density of moving grains and their velocity.

We can then write the grain born shear stress as proportional to the moving grain density  $n$  and to the drag force acting on a grain moving at the average velocity  $\bar{u}^p$  due to a flow at the velocity  $u$ :

$$\tau^p = n f_d \quad \text{with} \quad f_d = \frac{\pi}{8} C_d^\infty \rho_f (u - \bar{u}^p)^2 d^2. \quad (17)$$

Here, for the sake of the argument, we neglect the dependence of the drag coefficient on the particle Reynolds number (see Eq. 3). A key assumption now is that grains are in a steady motion, which means that the drag force  $f_d$  balances a resistive force due granular friction, collisions with the bed and viscous lubrication forces. These different dissipative mechanisms can be modeled as an overall effective friction force characterized by a friction coefficient  $\mu_d$ :

$$f_d = \frac{\pi}{6} \mu_d (\rho_p - \rho_f) g d^3. \quad (18)$$

We can furthermore express the fluid velocity  $u_d$  at the transport threshold by assuming that the hydrodynamic drag exerted on a static grain ( $u^p = 0$ ) has to overcome a static friction, characterized by a coefficient  $\mu_s$ :

$$u_d = \sqrt{\frac{4\mu_s}{3C_d^\infty} \left(\frac{\rho_p}{\rho_f} - 1\right) g d}. \quad (19)$$

For later use, we define the corresponding threshold Shields number  $\Theta_d$  as

$$\Theta_d = \frac{\rho_f u_d^2}{(\rho_p - \rho_f) g d}. \quad (20)$$

Combining the above equations it follows that the velocity difference between the grain and the flow is constant:

$$\bar{u}^p = u - \sqrt{\frac{\mu_d}{\mu_s}} u_d \quad (21)$$

We now assume that the transported grains do not disturb the flow. Then, the flow velocity around grains  $u$  must be proportional to the shear velocity, so that  $u/u_d = \sqrt{\Theta/\Theta_d}$  (see Fig. 6 (a) below). One therefore deduces:

$$\bar{u}^p = u_d \left( \sqrt{\frac{\Theta}{\Theta_d}} - \sqrt{\frac{\mu_d}{\mu_s}} \right). \quad (22)$$

This predicts that the grain velocity does not vanish at the threshold, if friction is lowered during motion ( $\mu_d < \mu_s$ ). The velocity at threshold  $u_d(1 - \sqrt{\mu_d/\mu_s})$  can be interpreted as the velocity needed by a grain to be extracted from the bed and entrained by the flow.

Saturation is reached when the fluid shear stress equals the transport threshold at the surface of the static bed i.e. when  $\tau^p = \rho_f u_*^2 - \tau_d$ . As consequence, the number of transported particles per unit area is solely determined by the excess shear stress:

$$n = \frac{\rho_f u_*^2 - \tau_d}{f_d} = \frac{\Theta - \Theta_d}{\frac{\pi}{6} \mu_d d^2}. \quad (23)$$

Finally, the saturated flux reads:

$$q_{\text{sat}} = \frac{u_d d}{\phi_b \mu_d} (\Theta - \Theta_d) \left( \sqrt{\frac{\Theta}{\Theta_d}} - \sqrt{\frac{\mu_d}{\mu_s}} \right). \quad (24)$$

Inserting the expression (19) of  $u_d$ , one gets the scaling law for the flux at large  $\Theta$ :

$$q_{\text{sat}} \propto \Theta^{3/2} \sqrt{\left(\frac{\rho_p}{\rho_f} - 1\right) g d^3}. \quad (25)$$

## B. A simple transport model for saltation

We now proceed in a similar manner for the aeolian saltation regime, following ideas initially proposed by Owen (1964) and Ungar & Haff (1987). In this regime, the motion of the grains is not confined to a thin layer at the surface of the bed. We consider an average grain trajectory, in which the particle takes off from the bed with the horizontal velocity  $\bar{u}_\uparrow^p$ , and comes back to it with a velocity  $\bar{u}_\downarrow^p$ , after a hop of length  $a$ . Some momentum is extracted from the wind flow by the grains to perform their jumps, so that the particle shear stress writes

$$\tau^p = \rho_p \phi_b \frac{\bar{u}_\downarrow^p - \bar{u}_\uparrow^p}{a} q_{\text{sat}}. \quad (26)$$

Now we use again the decomposition of the saturated flux as the product of the grain density  $n$  and the grain velocity  $\bar{u}^p$  (Eq. 14). Saturated transport corresponds to the balance  $\tau^p = \rho_f u_*^2 - \tau_d$  so that  $n$  still has the same form as in the bed-load case:

$$n = \frac{(\rho_p - \rho_f) g d}{f_d} (\Theta - \Theta_d), \quad (27)$$

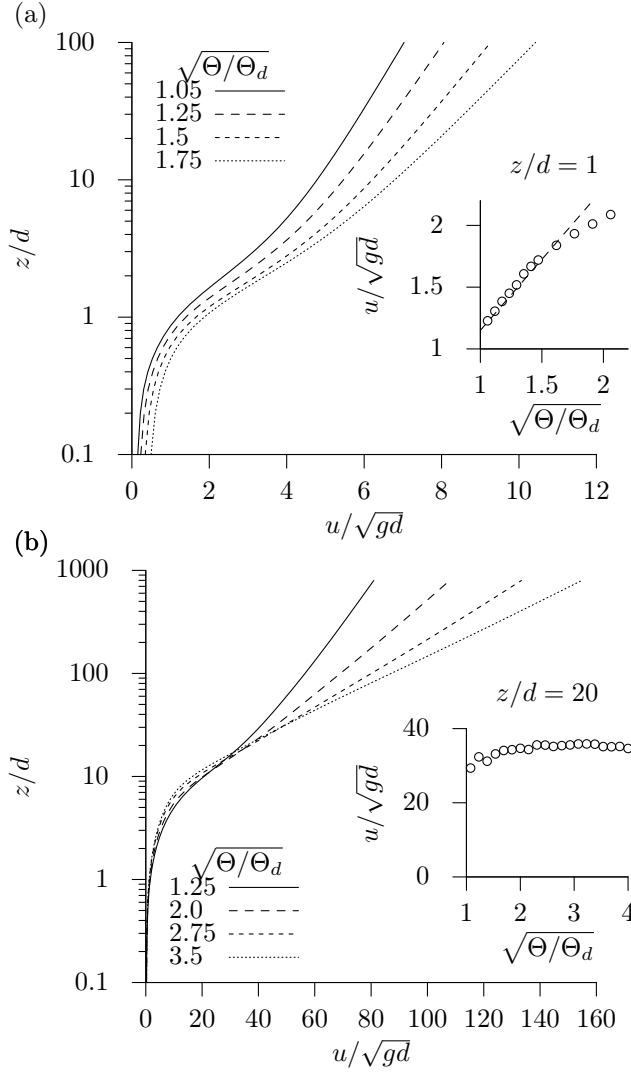


FIG. 6. Flow velocity vertical profiles at different shear velocity ratios  $\sqrt{\Theta/\Theta_d}$  for water (a) and air (b). Insets: velocity at  $z = d$  and  $z = 20d$  respectively, as a function of the rescaled shear velocity. The dashed line in the upper inset corresponds to the fit  $u \propto u_*$ .

but with a different effective drag force  $f_d$ , not related to friction anymore but to grain velocities. As the grain hop length can be related to the grain velocity as  $a \propto \bar{u}_\uparrow^p \bar{w}_\uparrow^p / g$  (ballistic approximation), we can effectively write

$$f_d \propto \frac{\pi}{6} d^3 \rho_p g \frac{\bar{u}_\downarrow^p - \bar{u}_\uparrow^p}{\bar{w}_\uparrow^p} \frac{\bar{u}^p}{\bar{u}_\uparrow^p}. \quad (28)$$

Now, for saltation, steady transport also implies that the number of grains expelled from the bed into the flow exactly balances those trapped by the bed, i.e. a replacement capacity equal to one. Due to the grain feedback on the flow, in contrast with bed load, grains in the transport layer feel a flow independent of the wind strength

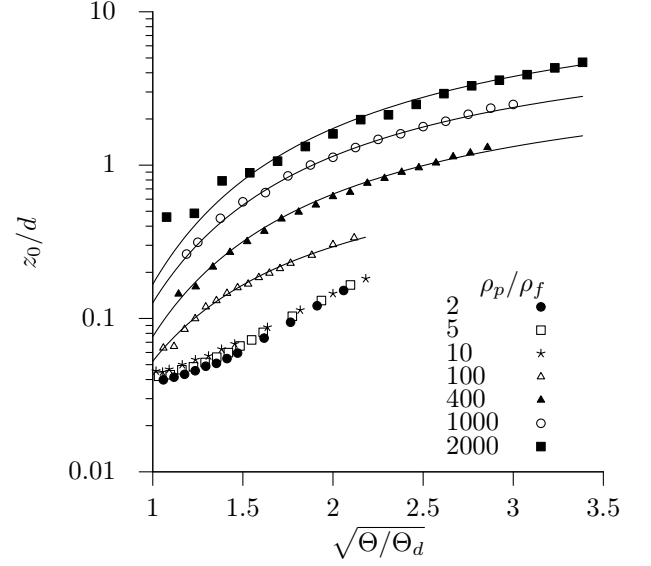


FIG. 7. Rescaled hydrodynamical roughness length as function of the shear velocity for different density ratios. Solid lines are the predictions based on the focal point assumption (Eq. 31).

(see Fig. 6 (b) below). Thus, new moving grains come only from high energy bed collisions. Since the number of ejected grains is a function of the impact energy (or equivalently, of the impact velocity), the mean grain velocity  $\bar{u}^p$  must be constant, independent of the shear velocity, scaling with  $u_d$ :

$$\bar{u}^p \propto u_d. \quad (29)$$

From this argument, it follows that all particle surface velocities ( $\bar{u}_\downarrow^p$ ,  $\bar{u}_\uparrow^p$ ,  $\bar{w}_\uparrow^p$ ) also scale with  $u_d$ , so that  $f_d$  is also a constant. Finally, the scaling law followed by the saturated flux becomes,

$$q_{\text{sat}} \propto (1 - \rho_f/\rho_p) u_d d (\Theta - \Theta_d). \quad (30)$$

### C. Comparison with simulations

The above simplifying models suggest a few simple tests to investigate the dynamical mechanisms in the DEM simulation. (i) Is saturation of transport due (or not) to the negative feedback of moving grains on the fluid? (ii) Do we recover the linear relation between the grain density  $n$  and the excess Shield number  $\Theta - \Theta_d$ , whatever the transport regime. (iii) Does the mean grain velocity  $u^p$  depend (or not) on the shear velocity?

#### 1. Grain feedback on the flow

The information of the feedback of moving grains on the fluid flow is formally encoded in the flow roughness



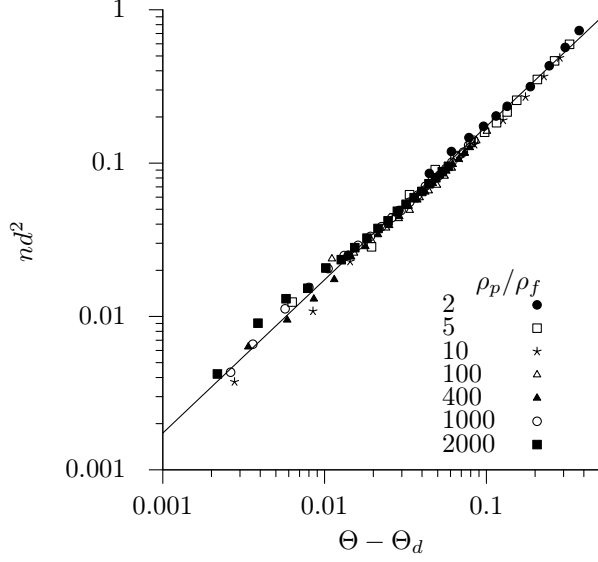


FIG. 8. Linear relation between the rescaled number of transported grains per unit area and the rescaled excess of shear stress for different density ratios.

length  $z_0$ . However, it can first be qualitatively understood from the shape of the flow velocity profile inside the transport layer (Fig. 6). For bed load, as shown in the inset of Fig. 6 (a), the flow velocity at  $z \simeq d$ , where most of transport takes place, increases with the shear velocity. This indicates that the flow is barely disturbed. In contrast, for aeolian transport (Fig. 6 (b)) the flow velocity is strongly affected by the motion of grains as it becomes almost independent of the wind in the region  $z \lesssim 20d$ , which accounts for most of the transport layer.

The data of the hydrodynamical roughness length  $z_0$  show a similar, or rather more complete, picture (Fig. 7). In the saltation regime the roughness length increases with the shear velocity as a result of grain feedback, which can be modeled from the existence of a focal point where  $u = U_f$  at  $z = H_f$  independently of  $u_*$  (Fig. 6 b), and above which the flow velocity recovers its log profile  $u = u_*/\kappa \ln(z/z_0)^{74,77,78}$ . This gives

$$z_0 \simeq H_f \exp(-\kappa U_f/u_*). \quad (31)$$

This expression reproduces well the increase of  $z_0$  for stronger winds, when the density ratio  $\rho_p/\rho_f$  is large enough (Fig. 7). Typically below  $\rho_p/\rho_f \simeq 10$ , Eq. 31 does not reproduce the data anymore. This is consistent with the absence of a focal point in the bed load regime (Fig. 6 a). Also, in the small  $\rho_p/\rho_f$  limit, the roughness length remains very small (substantially smaller than  $d$ ).

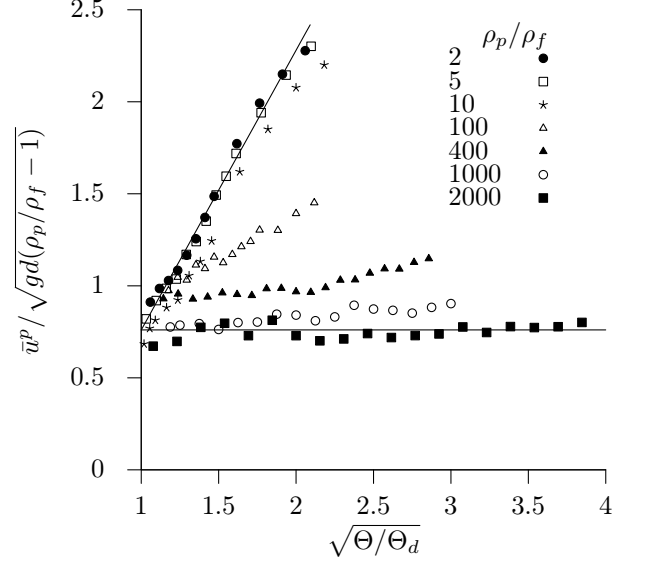


FIG. 9. Rescaled mean grain velocity as function of the rescaled the shear velocity for different density ratios. Full lines show the analytical prediction given in the text for the two limiting cases: water (Eq. 22) and air (Eq. 29).

## 2. Number of transported grains and average grain velocity

From expressions (15) and (16), we can compute the number of transported grains per unit area and the mean grain horizontal velocity as a function of the shear velocity of the flow. Figure 8 shows a linear relation between  $n$  and  $\Theta - \Theta_d$  for both bed load and saltation. This is consistent with the predictions of the above models. Interestingly, the friction coefficient  $\mu_d$ , defined from the proportionality factor (see Eq. 23), has the same value  $\simeq 1$  in both cases. This suggests that dissipation due to collisions of the moving grains with the bed plays the same role in both transport regimes.

The dependence of the mean grain velocity  $\bar{u}^p$  is also fully consistent with the picture emerging from the simple models. As shows in Fig. 9,  $\bar{u}^p$  increases linearly with  $\sqrt{\Theta/\Theta_d}$  for bed load (Eq. 22) while it remains roughly constant for aeolian saltation (Eq. 29). Interestingly, the different curves shown in Fig. 9 cross at  $\Theta = \Theta_d$ . In other words, the grain velocity at the transport threshold scale on  $\sqrt{gd(\rho_p/\rho_f - 1)}$ , with a prefactor slightly smaller than unity, whatever the transport regime. This common behavior between bed-load and saltation results from the fact that the negative feedback of transport on the flow disappears at the threshold, as  $n$  vanishes.

Fitting the grain density and the mean grain velocity to the simple model of bed load, one can extract the effective friction coefficients  $\mu_d$  and  $\mu_s$ . The static friction coefficient  $\mu_s$  turns out to be  $\simeq 4$  times larger than the dynamical friction coefficient  $\mu_d$ . This means that the

motion is lubricated by the fluid once the grains are entrained. Therefore, the grain velocity at the threshold remains finite (but  $n$  vanishes).

## V. SATURATION TRANSIENT

Beyond the properties of steady and homogeneous transport, we address in this section the time and length scales involved in the relaxation of the sediment flux toward its saturated value, which are relevant in the context of pattern formation<sup>79–84</sup>. We further emphasize the difference between the saturation time and the exchange time.

### A. Saturation length and time

Whatever the transport regime, the saturation transient is controlled by two mechanisms. On one hand, bed erosion or deposition must take place to adapt the number of transported grains to the flow velocity. On the other hand, grains must be accelerated by the flow to their asymptotic velocity.

We have addressed the case of saltation in a series of articles, starting from a controversy between us<sup>80,86,87</sup> and resolving it<sup>88</sup>. In summary, the horizontal acceleration of a grain entrained by the wind is governed by the equation of motion:

$$\frac{du^p}{dt} = \frac{3}{4} \frac{C_d^\infty \rho_f}{\rho_p d} (u - u^p)^2. \quad (32)$$

Contrary to bed load, in the saltation regime, dissipation only takes place during collisions and not through a permanent friction on the static bed. The only length scale in this equation is the so-called drag length  $\frac{\rho_p}{\rho_f} d$ . As a consequence, the relaxation of the particle velocity to the fluid velocity occurs over a length which varies as

$$L_{\text{sat}} \propto \frac{\rho_p}{C_d^\infty \rho_f} d, \quad (33)$$

independently of the wind speed, with a proportionality factor that depends on the restitution coefficient  $e$ <sup>73</sup>. Except in the vicinity of the transport threshold, the length over which the number of grains transported relaxes to its saturated state is much shorter than the drag length – it decays as  $1/u_*^2$ . Therefore, the overall saturation length is proportional to the drag length, as confirmed by direct measurements<sup>85</sup>.

The case of bed-load is still under debate<sup>39,54,83</sup>. We derive here the saturation time and the saturation length in the simple bed-load model detailed above. As the moving grains form a surface layer of thickness  $d$ , the number of moving particles per unit area adapts immediately to a change of shear velocity. By contrast, the grain velocity relaxes to its asymptotic value with a characteristic

time. This is what gives the saturation time. Neglecting the dependence of the drag coefficient on the particle Reynolds number, the horizontal component of the grain equation of motion reads:

$$\frac{du^p}{dt} = \frac{3C_d^\infty \rho_f}{4\rho_p d} \left[ (u - u^p)^2 - \frac{\mu_d}{\mu_s} u_d^2 \right]. \quad (34)$$

Linearising this equation around the asymptotic value, we obtain the following expression for the saturation time:

$$T_{\text{sat}} = \sqrt{\frac{\mu_s}{\mu_d}} \frac{2\rho_p d}{3C_d^\infty \rho_f u_d}. \quad (35)$$

Using expression (19) for  $u_d$  and typical values for the various parameters, we get  $T_{\text{sat}}$  on the order of few  $\sqrt{d/g}$ . The saturation length is then the length over which the grain moves during  $T_{\text{sat}}$  at velocity  $\bar{u}^p$ :

$$L_{\text{sat}} = \frac{2}{3} \frac{\rho_p d}{C_d^\infty \rho_f} \left( \sqrt{\frac{\mu_s}{\mu_d}} \frac{u}{u_d} - 1 \right). \quad (36)$$

Inserting again typical numbers in this expression, we get, for  $u$  close to  $u_d$ , a value for  $L_{\text{sat}}$  on the order of few grain diameters. This is consistent with indirect measurements of the saturation length based on the initial wavelength of sub-aqueous ripples<sup>83</sup>. Preliminary simulations of transport over a sinusoidal sand bed also confirm this order of magnitude.

### B. Exchange time vs saturation time

An important problem that cannot be tackled using the simple transport models presented here (or any Eulerian continuous model) is the exchange between the mobile and the static phases. Such models do not aim to describe the Lagrangian paths of individual grains. In particular, recent studies have focused on the characteristic time a given grain spends in the transport layer before being trapped by the bed<sup>39,54,83</sup>. This time, noted  $T_{\text{ex}}$  hereafter, is either called the deposition time or the exchange time. It is relevant in geology as it reflects the time scale associated with storage and reworking of sediments. The exchange time should *a priori* not be confused with the saturation time. Imagine for instance the case where all the grains in the transport layer would move with a uniform and perfectly horizontal velocity. Then there would be no exchange with the static phase and  $T_{\text{ex}}$  would be infinite, although transport could reach saturation after a very short time. Despite this conceptual difference, the formalism proposed in<sup>54</sup> leads to an identity between the exchange time and the saturation time.

Using our granular based transport simulations, we address this issue for bed load ( $\rho_p/\rho_f = 2$ ) by tracking all grains with velocities above a certain value at  $t = 0$ . For the sake of this discussion, we have chosen this value to

be  $\sqrt{gd}/2$ , which allows us to determine the grains inside the transport layer at the initial time. Noting this particle ensemble  $\mathcal{E}$ , we define the density  $n_t$  of moving grains at time  $t = 0$  that remains in the transport layer after a time  $t$ :

$$n_t = \frac{\left(\sum_{p \in \mathcal{E}} u_p\right)^2}{A \sum_{p \in \mathcal{E}} u_p^2}, \quad (37)$$

The time evolution of  $n_t$  in our numerical simulations is displayed in Fig. 10 (a). It can be seen that  $n_t(t)$  follows an exponential relaxation with time

$$n_t(t) = (n_0 - n_\infty) \exp(-t/T_{\text{ex}}) + n_\infty, \quad (38)$$

where  $n_0$  and  $n_\infty$  are the initial and asymptotic values, respectively. As the grains that no longer move have been exchanged with the static phase, the relaxation time of  $n_t$  is by definition the exchange time  $T_{\text{ex}}$ .

When analyzed for different shear velocities, the fraction of grains re-entrained in the flow after being trapped by the bed, which is given by the ratio  $n_\infty/n_0$  (Fig. 10 (b)), depends weakly on  $\sqrt{\Theta}$ . However, it seems to tend to zero at the threshold, which is a reasonable limit as all transported grains should be eventually trapped by the surface and replaced by new ones. The exchange time is also roughly constant, with a mean value  $T_{\text{ex}} \simeq 100\sqrt{d/g}$  (Fig. 10 (c)). This time is larger almost by two orders of magnitude than the saturation time. This means that exchange between the bed and the transport layer is not the dominant mechanism for the relaxation of the sediment flux towards saturation.

## VI. CONCLUSIONS

The aim of this paper was to present a novel numerical approach for sediment transport based on a discrete element method (DEM) for particles coupled to a continuum Reynolds averaged description of hydrodynamics. We have studied the effect of the grain to fluid density ratio  $\rho_p/\rho_f$  and showed that we can reproduce both (subaqueous) bed load at  $\rho_p/\rho_f$  close to unity, where transport occurs in a thin layer at the surface of the static bed, and (aeolian) saltation at large  $\rho_p/\rho_f$ , where the transport layer is wider and more dilute.

We have studied the mechanisms controlling steady, or saturated transport. In the bed load case, saturation is reached when the fluid borne shear stress at the interface between the mobile grains and the static grains is reduced to its threshold value. The number of grains transported per surface unit is therefore limited by the available momentum at the bed surface. However, the fluid velocity in the transport layer remains almost undisturbed so that the mean grain velocity scales with the shear velocity  $u_*$ . In the saltation case, particles in motion are able to eject others when they collide with the static bed, and saturation is reached when one grain is statistically replaced by

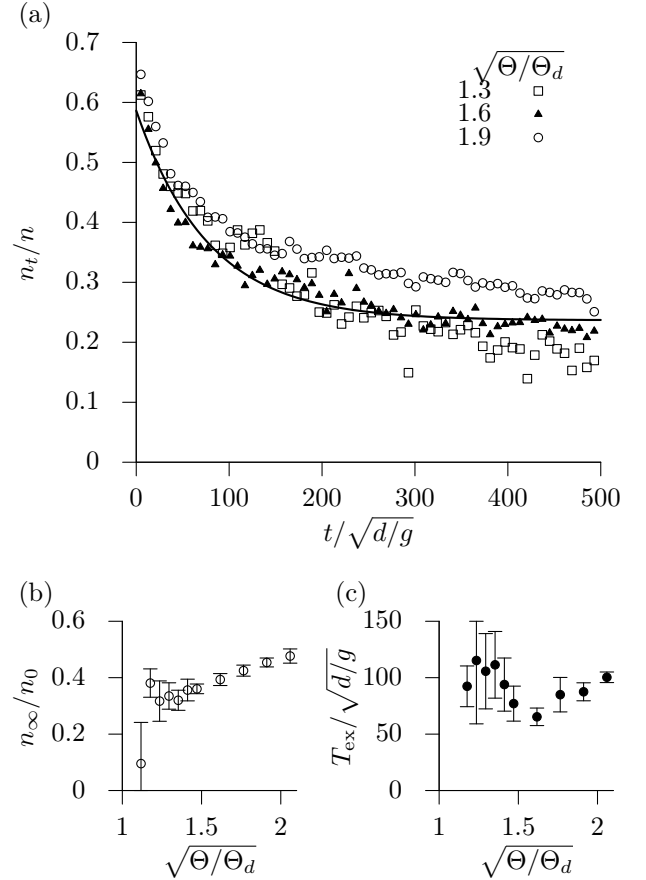


FIG. 10. (a) Time decay of the fraction of grains with an initial velocity above  $\sqrt{gd}/2$  that remain in the transport layer at time  $t$ , for different shear velocities. The solid line is the exponential fit (Eq. 38) of the data for  $\sqrt{\Theta/\Theta_d} = 1.6$  ( $\bullet$ ). Panels (b) and (c) respectively show the ratio of the asymptotic to initial value and the characteristic exchange time, as a function of the rescaled shear velocity.

exactly another one after collision. As a consequence, the mean grain velocity scales on the shear velocity threshold  $u_d$ , independently of  $u_*$ . This provides evidence for a strong negative feedback of the moving grains on the flow within the transport layer, where the wind velocity is reduced. In both bed load and saltation regimes, the number of grains transported per unit area is found proportional to the distance to threshold  $\Theta - \Theta_d$ , with an identical prefactor on the order of  $1/d^2$ .

We have systematically varied the density ratio in order to reveal the transition between these two transport regimes. This is also relevant for sediment transport in extraterrestrial atmospheres (Mars, Venus and Titan)<sup>82,89–91</sup>. We have shown that the properties of bed load transport are observed when  $s \lesssim 10$ , whereas those of aeolian saltation are well established when  $\rho_p/\rho_f$  is larger than few hundreds. Finally, we have discussed the saturation transient of sediment transport. Based on the mechanisms identified in the steady case, we have derived

expressions for the saturation time and length in the two regimes. In the bed load case, we have also shown that the exchange time, which reflects the time scale associated to exchange of particles between the mobile and static phases is two orders of magnitude larger than the saturation time.

This study could be continued in different directions. First, it would be interesting to look at the case where the bed is non erodible. This situation has been experimentally investigated in the aeolian regime<sup>92</sup>, showing a much wider transport layer  $\lambda$ , and new scaling laws for  $\lambda$ , the roughness  $z_0$  and the flux  $q_{\text{sat}}$  as a function of  $u_*$ . Further work should also be done to perform direct measurements of  $L_{\text{sat}}$  and  $T_{\text{sat}}$ . However, the study of inhomogeneous or unsteady situations requires a finer implementation of the model, especially for averaging procedures. A third axis is to take into account the turbulent fluctuations and to address the case of suspended transport<sup>93</sup>.

## ACKNOWLEDGMENTS

We thank Stefan Luding for kindly allowing us to use his MD code to simulate the granular system. We are also grateful to Jennifer Johnson for a careful reading of the manuscript. This work has benefited from the financial support of the Agence Nationale de la Recherche, grant 'Zephyr' (#ERCS07\_18).

- <sup>1</sup>L. F. Richardson, "Atmospheric diffusion shown on a distance-neighbour graph," *Proc. R. Soc. London A* **110**, 709–737 (1926).
- <sup>2</sup>H. Rouse, "Modern conceptions of the mechanics of fluid turbulence," *Trans. ASCE*, paper number 1965, 463–543 (1936).
- <sup>3</sup>V.A. Vanoni, "Transportation of suspended sediment by water," *Trans. ASCE* **111**, 67–133 (1946).
- <sup>4</sup>C. Crowe, M. Sommerfeld, and Y. Tsuji, "Multiphase Flows with Particles and Droplets", CRC Press, New York, 1998.
- <sup>5</sup>J. Bec, L. Biferale, M. Cencini, A. Lanotte, S. Musacchio and F. Toschi, "Heavy particle concentration in turbulence at dissipative and inertial scales," *Phys. Rev. Lett.* **98**, 084502 (2007).
- <sup>6</sup>F. Toschi and E. Bodenschatz, "Lagrangian properties of particles in turbulence," *Annu. Rev. Fluid Mech.* **41**, 375–404 (2009).
- <sup>7</sup>I. de Pater and J. Lissauer, "Planetary Science," (Cambridge University Press, Cambridge, 2001).
- <sup>8</sup>A. Kostinski and R. Shaw, "Scale-dependent droplet clustering in turbulent clouds," *J. Fluid Mech.* **434**, 389–398 (2001).
- <sup>9</sup>W.S. Chepil and R.A. Milne, "Comparative study of soil drifting in the field and in a wind tunnel," *Sci. Agric.* **19**, 149–257 (1939).
- <sup>10</sup>R.A. Bagnold, "The Physics of blown sand and desert dunes," Chapman and Hall, London, 1941.
- <sup>11</sup>A.W. Zingg, "Wind tunnel studies of movement of sedimentary material," *Proc. 5th Hydraulic Conference Bull.* **34**, 111–134 (1953).
- <sup>12</sup>G. Williams, "Some aspects of aeolian saltation load," *Sedimentology* **3**, 257–287 (1964).
- <sup>13</sup>J.N. Svasek and J.H.J. Terwindt, "Measurements of sand transport by wind on a natural beach," *Sedimentology* **21**, 311–322 (1974).
- <sup>14</sup>W.G. Nickling, "Eolian sediment transport during dust storms: Slims River valley, Yukon Territory," *Can. J. Earth Sci.* **15**, 1069–1084 (1978).
- <sup>15</sup>J.R. Jones and B.B. Willetts, "Errors in measuring aeolian flow by means of an adjustable trap," *Sedimentology* **26**, 463–468 (1979).
- <sup>16</sup>B.R. White, "Soil transport by winds on Mars," *J. Geophys. Res.* **84**, 4643–4651 (1979).
- <sup>17</sup>B.B. Willetts, M.A. Rice and S.E. Swaine, "Shape effects in aeolian grain transport," *Sedimentology* **29**, 409–417 (1982).
- <sup>18</sup>R. Greeley, D.G. Blumberg and S.H. Williams, "Field measurement of the flux and speed of wind blown sand," *Sedimentology* **43**, 41–52 (1996).
- <sup>19</sup>J.D. Iversen and K.R. Rasmussen, "The effect of wind speed and bed slope on sand transport," *Sedimentology* **46**, 723–731 (1999).
- <sup>20</sup>Anderson, R.S., Hallet, B., 1986. Sediment transport by wind: Toward a general model. *GSA Bulletin* **97**, 523–535.
- <sup>21</sup>R.S. Anderson and P.K. Haff, "Simulation of aeolian saltation," *Science* **241**, 820–823 (1988).
- <sup>22</sup>R.S. Anderson and P.K. Haff, "Wind modification and bed response during saltation of sand in air," *Acta Mechanica [Suppl.]* **1**, 21–51 (1991).
- <sup>23</sup>B.T. Werner, "A steady-state model of wind-blown sand transport," *J. Geol.* **98**, 1–17 (1990).
- <sup>24</sup>Kok, J.F., Renno, N.O., 2009. A comprehensive numerical model of steady state saltation (COMSALT). *J. Geophys. Res.* **114**, D17204.
- <sup>25</sup>R. Kawamura, "Study on sand movement by wind," *Reports of Physical Sciences Research Institute of Tokyo University* **5**, 95–112 (1951).
- <sup>26</sup>P.R. Owen, "Saltation of uniform grains in air," *J. Fluid Mech.* **20**, 225–242 (1964).
- <sup>27</sup>R.J. Kind, "A critical examination of the requirements of model simulation of wind induced erosion/deposition phenomena such as snow drifting," *Atmospheric Environment* **10**, 219–227 (1976).
- <sup>28</sup>K. Lettau and H.H. Lettau, "Experimental and micro-meteorological field studies of dune migration," In H.H. Lettau and K. Lettau eds., *Exploring the world's driest climate*, University of Wisconsin-Madison, Institute for Environmental studies, IES report 101, 110–147 (1978).
- <sup>29</sup>J.E. Ungar and P.K. Haff, "Steady state saltation in air," *Sedimentology* **34**, 289–299 (1987).
- <sup>30</sup>M. Sørensen, "An analytic model of wind-blown sand transport," *Acta Mechanica [Suppl.]* **1**, 67–81 (1991).
- <sup>31</sup>G. Sauermaann, K. Kroy and H.J. Herrmann, "A phenomenological dynamic saltation model for dune formation," *Phys. Rev. E* **64**, 031305 (2001).
- <sup>32</sup>E. Meyer-Peter and R. Müller, "Formulas for bed load transport," *Proc., 2nd Meeting, IAHR, Stockholm, Sweden*, 39–64 (1948).
- <sup>33</sup>H.A. Einstein, "The bed load function for sedimentation in open channel flows," *Technical bulletin (US Dept. of Agriculture)*, **1026**, 1–69 (1950).
- <sup>34</sup>R.A. Bagnold, "The flow of cohesionless grains in fluids," *Phil. Trans. R. Soc. Lond.* **249**, 235–297 (1956).
- <sup>35</sup>S. Yalin, "An expression for bed-load transportation," *J. Hydraul. Div. HY3*, 221–250 (1963).
- <sup>36</sup>J.S. Ribberink, "Bed-load transport for steady flows and unsteady oscillatory flows," *Coastal Eng.* **34**, 58–82 (1998).
- <sup>37</sup>B. Camenen and M. Larson, "A general formula for non-cohesive bed-load sediment transport," *Estuarine Coastal* **63**, 249–260 (2005).
- <sup>38</sup>M. Wong and G. Parker, "Reanalysis and correction of bed-load relation Meyer-Peter and Müller using their own database," *J. Hydraul. Eng.* **132**, 1159–1168 (2006).
- <sup>39</sup>E. Lajeunesse, L. Malverti and F. Charru, "Bedload transport in turbulent flow at the grain scale: experiments and modeling," *J. Geophys. Res.*, **115**, F04001 (2010).
- <sup>40</sup>R.A. Bagnold, "The nature of saltation and of bedload transport in water," *Proc. R. Soc. Lond. A* **332**, 473–504 (1973).
- <sup>41</sup>L.C. van Rijn, "Sediment transport, part I: bed-load transport," *J. Hydraul. Eng.* **110**, 1431–1456 (1984).
- <sup>42</sup>F. Engelund and J. Fredsøe, "A sediment transport model for straight alluvial channels," *Nordic Hydrology* **7**, 293–306 (1976).
- <sup>43</sup>P.L. Wiberg and J.D. Smith, "Model for calculating bed load transport of sediment," *J. Hydraul. Eng.* **115**, 101–123 (1989).

- <sup>44</sup>M. Sekine and H. Kikkawa, "Mechanics of saltating grains II", *J. Hydraul. Eng.* **118**, 536–558 (1992).
- <sup>45</sup>R. Fernandez Luque and R. van Beek, "Erosion and transport of bed-load sediment," *J. Hydraul. Res.* **14**, 127–144 (1976).
- <sup>46</sup>J.E. Abbot and J.R.D. Francis "Saltation and suspension trajectories of solid grains in a water stream," *Phil. Trans. R. Soc. Lond. A* **284**, 225–254 (1977).
- <sup>47</sup>Y. Niño, M. García and L. Ayala, "Gravel saltation. 1. Experiments," *Water Resources Res.* **30**, 1907–1914 (1994).
- <sup>48</sup>H.-Y. Lee and I.-S. Hsu, "Investigation of saltating particle motions," *J. Hydraul. Eng.* **120**, 831–845 (1994).
- <sup>49</sup>F. Charru, E. Larrieu, J.-B. Dupont and R. Zenit, "Motion of a particle near a rough wall in a viscous shear flow," *J. Fluid Mech.* **570**, 431–453 (2007).
- <sup>50</sup>J.K. McEwan, B.B. Willetts and M.A. Rice, "The grain/bed collision in sand transport by wind," *Sedimentology* **39**, 971–981 (1992).
- <sup>51</sup>P. Nalpanis, J.C.R. Hunt and C.F. Barrett, "Saltating particles over flat beds," *J. Fluid Mech.* **251**, 661–685 (1993).
- <sup>52</sup>J.-M. Foucaut and M. Stanislas, "Experimental study of saltating particle trajectories," *Exp. Fluids* **22**, 321–326 (1997).
- <sup>53</sup>X.-Y. Zou, Z.-L. Wang, Q.-Z. Hao, C.-L. Zhang, Y.-Z. Liu and G.-R. Dong, "The distribution of velocity and energy of saltating sand grains in a wind tunnel," *Geomorphology* **36**, 155–165 (2001).
- <sup>54</sup>Charru, F., 2006. Selection of the ripple length on a granular bed. *Phys. Fluids* **18**, 121508.
- <sup>55</sup>Cellino, M., 1998. Experimental Study of Suspension Flow in Open Channel. Doctoral dissertation No. 1824, Ecole Polytechnique Fdrale, Lausanne, Suisse.
- <sup>56</sup>Cellino, M., Lemmin, U., 1999. Coherent Flow Structure Analysis in Suspension Flows. XXVIII IAHR Congress, Graz, Austria.
- <sup>57</sup>Baas, A.C.W., 2004. Evaluation of Saltation Flux Impact Responders (Safires) for measuring instantaneous aeolian sand transport rates. *Geomorphology* **59**, 99–118.
- <sup>58</sup>Van Boxel, J.H., Sterk, G. & Arens, S.M., 2004. Sonic anemometers in aeolian sediment transport research. *Geomorphology* **59**, 131–147.
- <sup>59</sup>Baas, A.C.W. & Sherman, D.J., 2005. The formation and behavior of aeolian streamers. *Journal of Geophysical Research* **110**, F03011.
- <sup>60</sup>C. Marchioli, V. Armenio, M.V. Salvetti and A. Soldati 2006. Mechanisms for deposition and resuspension of heavy particles in turbulent flow over wavy interfaces. *Phys. Fluids* **18**, 025102.
- <sup>61</sup>Baas, A.C.W., 2008. Challenges in aeolian geomorphology: investigating aeolian streamers. *Geomorphology* **93**, 3–16.
- <sup>62</sup>Le Louvetel-Poilly, J., Bigillon, F., Doppler, D., Vinkovic, I., Champagne, J.-Y., 2009. Experimental investigation of ejections and sweeps involved in particle suspension. *Water Resour. Res.* **45**, W02416.
- <sup>63</sup>Ouriemi, M., Aussillous, P. and Guazzelli, E. 2009 Sediment dynamics. Part 1. Bed-load transport by laminar shearing flows, *J. Fluid Mech.* **636**, 295 - 319.
- <sup>64</sup>P.A. Cundall, and O.D.L. Strack, "A discrete numerical model for granular assemblies", *Géotechnique*, **29** 1, 47–65 (1979).
- <sup>65</sup>S. Luding, "Collisions and contacts between two particles", In: Herrmann H.J., Hovi J.P., Luding S. (eds) *Physics of dry granular media - NATO ASI Series E350*, Kluwer Academic Publishers, Dordrecht, 285 (1998).
- <sup>66</sup>S. Luding, "Cohesive, frictional powders: contact models for tension", *Granular matter* **10**, 4 (2008).
- <sup>67</sup>*Discrete-element Modeling of Granular Materials*, Edited by F. Radjaï and F. Dubois, ISTE, Wiley, 2011.
- <sup>68</sup>R.I. Ferguson and M. Church, "A simple universal equation for grain settling velocity," *J. Sedim. Res.* **74**, 933–937 (2004).
- <sup>69</sup>Prandtl, L., 1925. Bericht über Untersuchungen zur ausgebildeten Turbulenz. *Zeitschrift für angewandte Mathematik und Mechanik*, **5**, 136–139.
- <sup>70</sup>Shields, A., 1936. Application of similarity principles and turbulence research to bed-load movement. *Mitteilungen der Preussischen Versuchsanstalt für Wasserbau und Schiffbau* **26**, 5–24.
- <sup>71</sup>Rasmussen, K.R., Iversen, J.D., Rautheimo, P., 1996. Saltation and wind flow interaction in a variable slope wind tunnel. *Geomorphology* **17**, 19–28.
- <sup>72</sup>Rasmussen, K.R., Mikkelsen, H.E., 1991. Wind tunnel observations of aeolian transport rates. *Acta Mechanica [Suppl]* **1**, 135–144.
- <sup>73</sup>B. Andreotti, "A two species model of aeolian sand transport," *J. Fluid Mech.* **510**, 47–50 (2004).
- <sup>74</sup>Creysse, M., Dupont, P., Ould el Moctar, A., Valance, A., Cantat, I., Jenkins, J.T., Pasini, J.M., Rasmussen, K.R., 2009. Saltating particles in a turbulent boundary layer: experiment and theory. *J. Fluid Mech.* **625**, 47–74.
- <sup>75</sup>Quartier, L., Andreotti, B., Daerr, A., Douady, S., 2000. Dynamics of a grain on a sandpile model. *Phys. Rev E* **62**, 8299–8307.
- <sup>76</sup>B. Andreotti, 2007. A mean field model for the rheology and the dynamical phase transitions in the flow of granular matter, *Europhys. Lett.* **79**, 34001.
- <sup>77</sup>Liu, X., Dong, Z., 2004. Experimental investigation of the concentration profile of a blowing sand cloud. *Geomorphology* **60**, 371–381.
- <sup>78</sup>Rasmussen, K.R., Sorensen, M., 2008. Vertical variation of particle speed and flux density in aeolian saltation: Measurement and modeling. *J. Geo. Res.* **113**, F02S12, doi:10.1029/2007JF000774.
- <sup>79</sup>Andreotti, B., Claudin, P., Douady, S., 2002. Selection of barchan shapes and velocities. Part 1: Dynamics of sand, wind and dunes, *Eur. Phys. J. B* **28**, 321–339.
- <sup>80</sup>Andreotti, B., Claudin, P., Douady, S., 2002. Selection of barchan shapes and velocities. Part 2: A two-dimensional modelling, *Eur. Phys. J. B* **28**, 341–352.
- <sup>81</sup>Hersen, P., Douady, S., Andreotti, B., 2002. Relevant lengthscale of barchan dunes. *Phys. Rev. Lett.* **89**, 264301.
- <sup>82</sup>Claudin, P., Andreotti, B., 2006. A scaling law for aeolian dunes on Mars, Venus, Earth, and for subaqueous ripples. *Earth Planet. Sci. Lett.* **252**, 30–44.
- <sup>83</sup>Fourrière, A., Claudin P., Andreotti, B., 2010. Bedforms in a turbulent stream: formation of ripples by primary linear instability and of dunes by non-linear pattern coarsening. *J. Fluid Mech.* **649**, 287–328.
- <sup>84</sup>B. Andreotti, P. Claudin, O. Devauchelle, O. Durán and A. Fourrière, 2011 Bedforms in a turbulent stream: ripples, chevrons and antidunes, to appear in *J. Fluid Mech.*
- <sup>85</sup>Andreotti, B., Claudin, P., Pouliquen, O., 2010. Measurements of the aeolian sand transport saturation length. *Geomorphology*, **123**, 343–348.
- <sup>86</sup>Durán, O., Herrmann, H.J., 2006. Modeling of saturated sand flux. *J. Stat. Mech.* P07011.
- <sup>87</sup>Parteli, E.J.R., Durán, O., Herrmann, H.J., 2007. Minimal size of a barchan dune. *Phys. Rev. E* **75**, 011301; Reply to comment on 'Minimal size of a barchan dune'. *Phys. Rev. E* **76**, 063302.
- <sup>88</sup>Durán, O., Claudin, P. and Andreotti, B. 2011 On aeolian transport: grain-scale interactions, dynamical mechanisms and scaling laws. To appear in *Aeolian Research*.
- <sup>89</sup>Almeida, M.P., Parteli, E.J.R., Andrade, J.S., Herrmann, H.S., 2008. Giant saltation on Mars. *PNAS* **105**, 479–495.
- <sup>90</sup>Andreotti B, 2008 Contradictory saltation height measurements and unphysical assumptions. Comment on "Giant saltation on Mars." by Almeida, M.P., Parteli, E.J.R., Andrade, J.S., Herrmann, H.S. *PNAS* **105** E60.
- <sup>91</sup>Kok, J.F., 2010. Difference in the wind speeds required for initiation versus continuation of sand transport on Mars: Implications for dunes and dust storms. *Physical Review Letters*, **104**, 074502.
- <sup>92</sup>Ho, T.D., Valance, A., Dupont, P., Ould El Moctar, A., 2011. Scaling laws in aeolian sand transport. *Physical Review Letters*, **106**, 094501.
- <sup>93</sup>Claudin, P., Charru, F., Andreotti, B., 2011. Transport relaxation time and length scales in turbulent suspensions. *J. Fluid Mech.* **671**, 491–506.